A Quadratic Energy Minimization Framework for Signal Loss Estimation from Arbitrarily Sampled Ultrasound Data*

Christoph Hennersperger[1], Diana Mateus[1,2], Maximilian Baust[1], and Nassir Navab[1]

[1] Computer Aided Medical Procedures, Technische Universität München, Germany
[2] Institute of Computational Biology, Helmholtz Zentrum München, Germany
christoph.hennersperger@tum.de

Abstract. We present a flexible and general framework to iteratively solve quadratic energy problems on a non uniform grid, targeted at ultrasound imaging. Therefore, we model input samples as the nodes of an irregular directed graph, and define energies according to the application by setting weights to the edges. To solve the energy, we derive an effective optimization scheme, which avoids both the explicit computation of a linear system, as well as the compounding of the input data on a regular grid. The framework is validated in the context of 3D ultrasound signal loss estimation with the goal of providing an uncertainty estimate for each 3D data sample. Qualitative and quantitative results for 5 subjects and two target regions, namely US of the bone and the carotid artery, show the benefits of our approach, yielding continuous loss estimates.

1 Introduction

Many algorithms in computer vision and image processing, such as diffusion image filtering [7] or random walks for image segmentation [1], require the minimization of quadratic energy terms of the form

$$E(x) = \frac{1}{2}x^T Ax - x^T b, \tag{1}$$

where $x \in \mathbb{R}^m$ denotes the solution vector, given a positive definite system matrix $A \in \mathbb{R}^{m \times m}$ and a vector $b \in \mathbb{R}^m$. Such energies are usually defined on a graph shaped as a square lattice resembling the spatial structure of the image data. However today, and especially in medical imaging, the concept of an image extends to sensor readings that sample the space arbitrarily, e.g. in SPECT and ultrasound data. For the latter, single 1D rays, so-called *scanlines*, are processed independently and get converted into 2D images subsequently. This scan-conversion step is based on the transducer geometry, which is often non-rectangular, e.g. in case of curvilinear or phased-array transducers. Furthermore,

* This work was partially supported by the EU 7th Framework, No. 270460 (ACTIVE), and the Bavarian state program Leitprojekte Medizintechnik (BayMED).

P. Golland et al. (Eds.): MICCAI 2014, Part II, LNCS 8674, pp. 373–380, 2014.

the image planes of 3D freehand sweeps are hardly parallel, as straight trajectories are difficult to maintain. Therefore, the irregularly sampled data is usually *compounded* prior to further processing, i.e. image intensities are interpolated w.r.t. a rectangular grid. We argue that for the minimization of a quadratic energy involving US data, such as for segmentation [1], signal loss estimation (SLE) [3], or Speckle reduction [8], compounding is not only unnecessary, but also counterproductive, as interpolation can imply a potential loss of information [4]. The main contribution of this work is therefore a framework for solving arbitrary quadratic energy minimization problems in a ray-based and thus compounding-free manner. Moreover, we propose an ultrasound-specific construction of directed graphs allowing for the definition of direction and potential dependent edge weights (e.g. weights that resemble the direction of propagation of the US rays). The aforementioned generalizations pose additional challenges: i) A specialized neighbor search is required, as a straightforward nearest neighbor (NN) search does not reflect the US specific image formation process. ii) The symmetry and the linearity of Eq. (1) are not necessarily preserved, which requires adaption of the employed optimization algorithms. In this regard, there has been previous work where most relevant is the one of Singaraju *et al.* [5], who employed a Newton-descent like iterative algorithm. Here, we also propose to deal with the problem in an iterative fashion using a modified version of the conjugate gradient method, with re-initialization, cf. Sec. 2.

To demonstrate its applicability, the proposed framework is used for signal loss estimation in three-dimensional US sweeps, where a value of "confidence" is estimated for each pixel following a random walker formulation [3], cf. Sec. 3. As observed in Fig. 1 and in contrast to the proposed method, the naive application of the approach of [3], either frame-wise, or via a compounding, leads to either discontinuities, or compounding-related artifacts in frame direction, respectively. Thanks to the construction of a directed graph network on the spatially irregular samples and through the proper definition of graph weights, our method instead achieves continuity along the trajectory.

2 Quadratic Energies on Irregular Ultrasound Graphs

The proposed framework consists of two main steps: i) building a connected graph from arbitrary US samples in 3D space, and ii) making use of this graph structure to effectively minimize quadratic energy terms in an iterative update scheme directly on the graph.

Directed Graph-Network for 3D Ultrasound. For 3D ultrasound data, a graph can be constructed from either a *compounded* dataset or directly from the original ultrasound samples lying in 3D space. Although the graph construction is easier in the former case, the latter is by far better suited to ultrasound data, as in US imaging, single 1D rays are acquired independently. With an irregular graph built from individual samples in 3D space, minimization problems can be solved efficiently, yielding results directly corresponding to the input data.

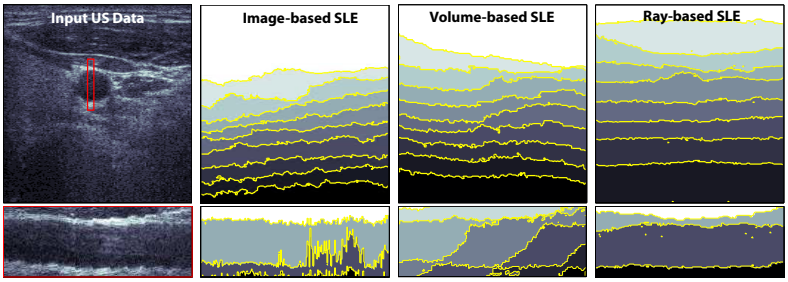

Fig. 1. Signal Loss Estimation for Carotid Artery 3D US From left to right: Original ultrasound data, loss estimates obtained by a frame-based and a compounding-based application of [3], as well as our method. Shaded areas show confidence values quantized into 10 equidistant steps. The red window in the US image marks the longitudinal view shown in the second row. It can be clearly observed that ray-based SLE are the most consistent along the sweep direction.

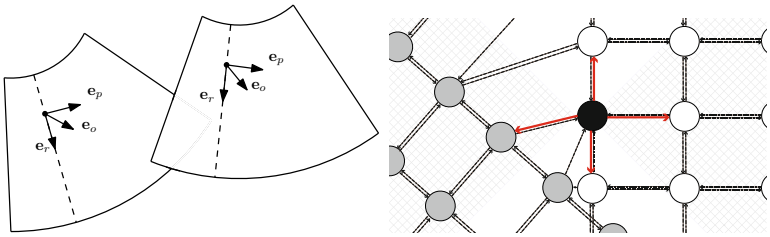

Fig. 2. Graph construction from two views, simplified to a 2D plane. **Left:** Two views with exemplary local coordinate systems defining the orthants. **Right:** Graph constructed from the two views (white and grey nodes) at their intersection area. The bold red arrows show all *outgoing* edges from one specific node (black), and the grey grid areas indicate the orthants for the marked node.

Thus, we aim to construct a graph directly from K arbitrarily spaced US rays (*scanlines*), where each of them consists of N ultrasound sampling points. The sampling points will be denoted by $\boldsymbol{x}_{k,l} \in \mathbb{R}^3$ with corresponding intensity values $I_{k,l}$, where $k = 1, \ldots, K$ and $l = 1, \ldots, N$. Each of these sampling points will be associated to a node n_i ($i = 1, \ldots, M$; $M = KN$) in the graph $\mathcal{G} = (\mathcal{N}, \mathcal{E}, \mathcal{W})$, where $\mathcal{N}$, $\mathcal{E}$, and $\mathcal{W}$ denote the set of nodes, edges, and weights, respectively. Further, we introduce the bijection

$$\Theta : \{1, \ldots, N\} \times \{1, \ldots, K\} \to \{1, \ldots, M\}, \quad (k, l) \mapsto i = \Theta(k, l) \tag{2}$$

in order to number all nodes. We call two nodes n_i and n_j *connected* if there exists an edge $e_{i,j}$ or $e_{j,i}$ in $\mathcal{E}$. It is important to note that we construct a *directed* graph, as ultrasound imaging is directional by nature with ultrasonic waves traversing through tissue originating from the transducer. Thus we explicitly make a difference between $e_{i,j}$ going from n_i to n_j and $e_{j,i}$ going from n_j to n_i. Each node

is connected to six neighbors via *six outgoing* edges. As US samples are lying arbitrarily in 3D space, a naive nearest neighbor search does not resemble the US-specific image formation process. Thus, we propose a different approach and endow every node (or equivalently every sampling point) with a local coordinate system which is given by the orthonormal vectors $\boldsymbol{e}_r, \boldsymbol{e}_p, \boldsymbol{e}_o \in \mathbb{R}^3$, cf. Fig. 2. The vector $\boldsymbol{e}_r$ is pointing into the direction of the ray, $\boldsymbol{e}_p$ is orthogonal to it and lies within the acquisition plane, and $\boldsymbol{e}_o$ is orthogonal to both of them. Given a node n_i we can now define its six neighboring nodes as follows. At first we connect it to its upper and lower neighbors n_U and n_L w.r.t. the scan line direction $\boldsymbol{e}_d$. Let $(k,l) = \Theta^{-1}(i)$, then $n_U = n_{\Theta(k,l-1)}$, and $n_L = n_{\Theta(k,l+1)}$. Based on $\boldsymbol{e}_p$ and $\boldsymbol{e}_o$ we define the four orthants

$$\Omega_N = \left\{(k',l') : \boldsymbol{e}_o = \arg\min_{\boldsymbol{p}=\pm\boldsymbol{e}_o,\pm\boldsymbol{e}_p} \angle(\boldsymbol{x}_{k',l'} - \boldsymbol{x}_{k,l}, \boldsymbol{p})\right\}, \tag{3}$$

$$\Omega_S = \left\{(k',l') : -\boldsymbol{e}_o = \arg\min_{\boldsymbol{p}=\pm\boldsymbol{e}_o,\pm\boldsymbol{e}_p} \angle(\boldsymbol{x}_{k',l'} - \boldsymbol{x}_{k,l}, \boldsymbol{p})\right\}, \tag{4}$$

$$\Omega_E = \left\{(k',l') : \boldsymbol{e}_p = \arg\min_{\boldsymbol{p}=\pm\boldsymbol{e}_o,\pm\boldsymbol{e}_p} \angle(\boldsymbol{x}_{k',l'} - \boldsymbol{x}_{k,l}, \boldsymbol{p})\right\}, \tag{5}$$

$$\Omega_W = \left\{(k',l') : -\boldsymbol{e}_p = \arg\min_{\boldsymbol{p}=\pm\boldsymbol{e}_o,\pm\boldsymbol{e}_p} \angle(\boldsymbol{x}_{k',l'} - \boldsymbol{x}_{k,l}, \boldsymbol{p})\right\}, \tag{6}$$

in which we aim to find the nearest neighbors in the different search directions and choose n_N, n_S, n_E, and n_W as the nodes corresponding to the samples with minimal Euclidean distance to $\boldsymbol{x}_{k,l}$ within the corresponding orthants. The orthants can be seen as search regions defined by the coordinate quadrant bisections, which are used to find neighbors orthogonal to the rays. It is important to note that the search in these local spaces results in an irregular directed graph, as for different local coordinates, neighbors will be found differently (see Fig. 2).

Minimization of Quadratic Energies on a Directed Graph. Recall that the minimization of the general quadratic energy in (1) corresponds to solving the equation system $Ax = b$, where A represents the graph Laplacian. In order to do so, we propose a meta-algorithm that can be combined with any iterative solution technique, which only requires a method implementing the matrix-vector multiplication Ax, such as the well-known conjugate gradient method. We note that the solution vector x contains the so-called node potentials defined by $p_i = P(n_i)$, where $P : \mathcal{N} \to [0,1]$, and the interpretation of these potentials depends on the application (cf. Sec. 3). In order to derive a method implementing Ax, we first introduce the directional derivatives w.r.t. its local neighborhood

$$\nabla_\xi p_i := p_\xi - p_i, \quad \text{where} \quad \xi \in \mathfrak{N}_i = \{U, L, N, S, E, W\}. \tag{7}$$

This definition allows us to write the directed and potential dependent graph Laplacian (corresponding to $\mathcal{G}$) at p_i as

$$\Delta p_i = \sum_{\xi \in \mathfrak{N}_i} \left[\mathbf{1}(p_i > p_\xi) w_{i\xi} + \mathbf{1}(p_i \leq p_\xi) w_{\xi i}\right] \nabla_\xi p_i, \tag{8}$$

where $\mathbf{1}(p_i > p_\xi) = 1$, if $p_i > p_\xi$, and $\mathbf{1}(p_i > p_\xi) = 0$ otherwise, which activates or deactivates the directed edges based on sign of the potential difference. The computation of Δp_i can be parallelized and thus efficiently implemented on a GPU.

As Δp_i corresponds to the $i-$th row of Ax, the proposed operation essentially represents a GPU-based *black box* for this matrix vector multiplication. The next step for solving (1) consists now of selecting an appropriate iterative solver which can be combined with the aforementioned black box. An obvious, but slow candidate would be a classical gradient descent, i.e., $x^{t+\tau} = x^t - \tau(Ax^t - b)$. In contrast to this, we employed a conjugate gradient method.

It is important to note that in case of a regular grid of voxels, symmetric edge weights, and no dependency on the potentials, the corresponding graph Laplacian A would be symmetric positive definite. Thus, the plain application of the conjugate gradient method would already be sufficient for minimizing (1). The symmetry of A is, however, not preserved in the case of potential-dependent edge weights in a directed graph. From a theoretical point of view, this would prohibit the application of the conjugate gradient method without any further modification. Thus, we propose to augment the selected iterative solver, in our case the CG method, with an additional outer iteration loop. For each outer cycle, a set of active edges is determined by evaluating the indicator function in (8) once for the whole graph. This set of active edges is then kept constant for the next η iterations of each inner cycle, where the CG update scheme is started from the initial node potentials first and then updated accordingly with the result of the previous cycle. As for the normal descent-like approach, the update-scheme is repeated until the residual is below a threshold ϵ. We found experimentally[1] that this procedure yields satisfactory results, as demonstrated in Fig. 3 and Fig. 4.

3 Signal Loss Estimation from Ultrasound

We show how the proposed framework can be applied to the specific task of signal loss (or uncertainty) estimation for 3D ultrasound imaging, where the goal is to retrieve a coefficient describing the reliability of the ultrasound signals at the different sample positions. The reliability of the ultrasound signal drops with depth as the signal is attenuated and absorbed in tissue. However, it is also partially scattered at small interfaces, and thus the reliability is also depending on neighboring tissue and surrounding interfaces. Although similar to attenuation estimation, signal loss estimates do not represent an absolute value, but the *relative confidence* of the correspdonding sample, in reference to a certainty of 100% at zero depth. As the SLE are retrieved globally for the whole acquisition, application fields for these values are extensive, with the most obvious ones being visualization, registration and segmentation of ultrasound data, where the values can be directly incorporated as a weighting term based on the confidence values assigned to the ultrasound samples.

The first step to use the proposed framework is to define weights and border conditions, such that the result of the minimization scheme yields a mapping of every ultrasound sample position to a reliability factor $\in [0, 1]$. The edge weights

[1] We also conducted experiments with the fast Jacobi method proposed by [2], but results were less convincing.

w_{ij} are defined to model ultrasound properties in an effective way, as inspired by [3]. To account not only for varying distances between connected nodes, but also for different incision angles of the ultrasound beams, we additionally make use of the unit vector $\boldsymbol{e}_r$, indicating the direction of every US ray, to evaluate the angles between compared nodes. This essentially accounts for the inherent directionality of ultrasound, where signals are similar for ray orientations which are parallel, but represent complementary information for rays which are perpendicular to each other. We define our weighting function as

$$w_{\xi i} = exp\left[-\left(\frac{|I_{\theta^{-1}(\xi)} - I_{\theta^{-1}(i)}|}{\sigma} + \gamma(|\boldsymbol{x}_{\theta^{-1}(\xi)} - \boldsymbol{x}_{\theta^{-1}(i)}|(1 - \langle \boldsymbol{e_r}^{\xi}, \boldsymbol{e_r}^{i} \rangle)\right)\right], \tag{9}$$

where σ controls the edge weight based on the image information, γ is a penalty for nodes with high distances and inter-scanline angles, and $\boldsymbol{e_r}^{i}$ is the ray direction for node i, extending the weights in [3] to arbitrary samples in space.

For the resulting loss estimates, it is known a priori that the relative signal strength at the transducer surface should be 1, while it is expected to be ≈ 0 for all regions which are outside of the US image in axial direction. To model this conditions, two virtual nodes n_t and n_s, the transducer (source) and sink, with $p_t = 1, p_s = 0$, are added [3]. To account for these virtual nodes, the right hand side b in (1) is initialized with zeros except for the the entries corresponding to the first row which are initialized with $b_{\Theta(k,1)} = -w_{N\Theta(k,1)}$ in order to satisfy the transducer-related boundary conditions. With these constraints in place, we calculate all weights for the edges constructed during graph setup, and apply the optimization scheme presented in the last section to retrieve a global solution for all undefined node potentials, representing the desired loss estimates.

4 Results and Discussion

We provide qualitative and quantitative results for SLE in case of 3D freehand ultrasound based on the presented framework for ultrasound scans of the carotid arteries, as well as the femoral bone. While in the former case, the lumen of the vessel is mostly surrounded by soft tissue, bone structures are strong reflectors which should result in clear steps in the signal loss estimates. For both applications, we acquired 5 datasets from different subject, each with a freehand US setup consisting of an Ultrasonix RP scanner providing scanline data coupled with an Ascension electromagnetic tracking device.

In terms of a quantitative evaluation, we compare estimates obtained using our approach to a method for uncertainty estimation from linear 2D ultrasound images [3] and to an extension of this method, which is applied on a volumetric (compounded) grid, where we used a backward-warping algorithm [6] prior to loss estimation. Qualitative results for exemplary cases are shown in Fig. 1 for the carotid artery, and in Fig. 3 for the femoral bone. We manually extract centerlines for the target structures of interest (carotid artery / bone) and evaluate the standard deviation of the extracted loss values along the acquired trajectories,

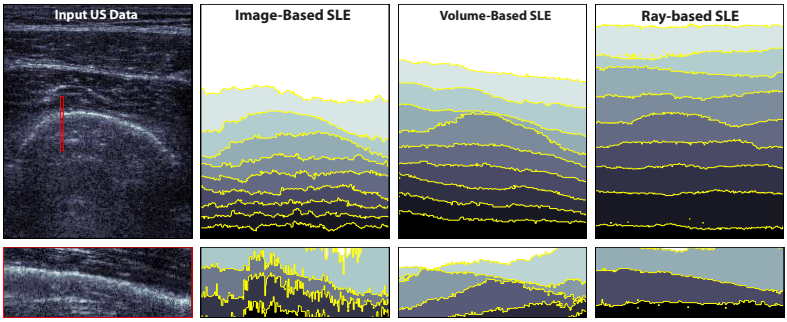

Fig. 3. Loss Estimates for Bone Ultrasound As for the carotid datasets (cf. Fig. 1), cross-sectional and longitudinal slices for the compared methods (second and third column) exhibit a strong variation for image and volume bases estimates, while our ray-based method provides consistent estimates, properly modeling the bone structure also in elevational direction.

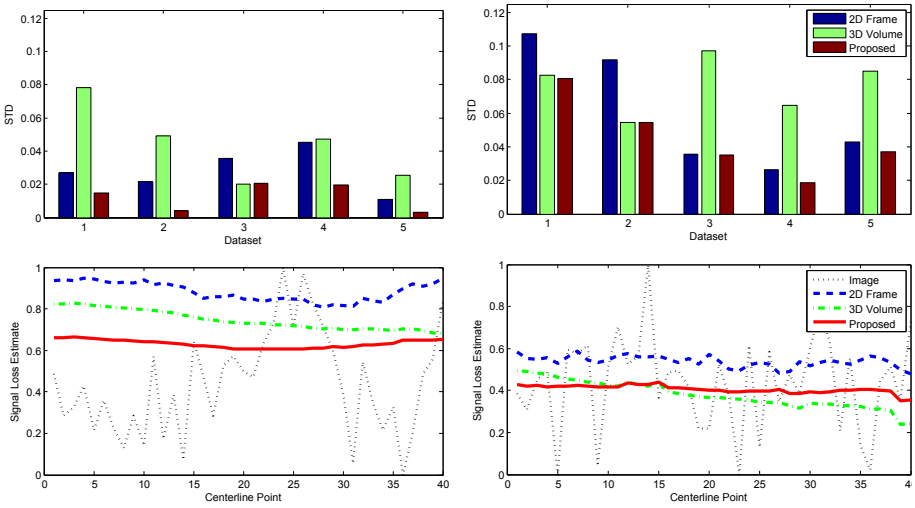

(a) Carotid Artery (b) Bone

Fig. 4. SLE Variations along centerlines The first row shows the standard deviations of SLE based on 2D images (blue), 3D volumetric (green) and 3D ray based (red) methods, respectively. The second row shows the actual SLE values for all methods along the centerline for carotid and femoral bone datasets 4.

as these should stay constant within the target structures. Fig. 4 shows the deviations of SLE values for the individual datasets, for which the standard deviation of all analyzed carotid records yields 0.00144 for the proposed method compared to 0.0483 and 0.0300 for volume and frame based approaches, as well as 0.0487 compared to 0.0780 and 0.0657 for the bone datasets.

The results show that our method provides continuous results, modeling target structures better than the two compared methods. In regard of the applicability of our proposed framework, the results show that the graph-structure is well-suited for its application to ultrasound, and may yield better performance due to avoiding compounding of the data. Besides the presented application, other fields can be directly considered, where the already mentioned SRAD [8] and graph-based segmentation [1] are just two examples.

5 Conclusion

While today, processing methods reyling on compounding-based US are still common, interpolation of the data on a regular grid is unneccessary and potentially destroys useful information. In this work, we presented a completely compounding-free optimization framework for general quadratic energies. By constructing an irregular, directed graph from the ultrasound data, US-specific properties can be modeled effectively, as shown for the application of signal loss estimation. Our proposed optimization scheme is directly applied on the graph structure in a parallel fashion and thus facilitates the global optimization of energies in an efficient way. As the framework enables a fast adaption to other problems in ultrasound imaging, we hope that this work helps to start a paradigm change to fully compouding-free processing of ultrasound data. Future research might include the application of this technique to other modalities comprising irregular sampling, as well as the investigation of different iterative solvers.

References

1. Grady, L.: Random walks for image segmentation. IEEE Transactions on Pattern Analysis and Machine Intelligence 28(11), 1768–1783 (2006)
2. Grewenig, S., Weickert, J., Schroers, C., Bruhn, A.: Cyclic schemes for pde-based image analysis. Tech. rep., Technical Report 327, Department of Mathematics, Saarland University, Saarbrücken, Germany (2013)
3. Karamalis, A., Wein, W., Klein, T., Navab, N.: Ultrasound confidence maps using random walks. Medical Image Analysis 16(6), 1101–1112 (2012)
4. Prager, R., Gee, A., Treece, G., Berman, L.: Freehand 3D ultrasound without voxels: volume measurement and visualisation using the stradx system. Ultrasonics 40(18), 109–115 (2002)
5. Singaraju, D., Grady, L., Vidal, R.: Interactive image segmentation via minimization of quadratic energies on directed graphs. In: IEEE Conference on Computer Vision and Pattern Recognition, CVPR 2008, pp. 1–8 (June 2008)
6. Solberg, O.V., Lindseth, F., Torp, H., Blake, R.E., Nagelhus Hernes, T.A.: Freehand 3d ultrasound reconstruction algorithmsa review. Ultrasound in Medicine and Biology 33(7), 991–1009 (2007)
7. Weickert, J., Romeny, B.M.T.H., Viergever, M.A.: Efficient and reliable schemes for nonlinear diffusion filtering. IEEE Transactions on Image Processing 7(3), 398–410 (1998)
8. Yu, S.T.Y., Acton: Speckle reducing anisotropic diffusion. IEEE Transactions on Image Processing 11(11), 1260–1270 (2002)